

Effect of Pore Size on Adsorption of a Polyelectrolyte to Porous Glass

Yael G. Mishael,^{*,†} Paul L. Dubin,^{*,‡} Renko de Vries,[§] and A. Basak Kayitmazer[‡]

Seagram Center for Soil and Water Sciences, Faculty of Agricultural Food and Environmental Sciences, Hebrew University of Jerusalem, Rehovot, Israel, Department of Chemistry, University of Massachusetts, Amherst, Massachusetts 01003, and Laboratory of Physical Chemistry and Colloid Science, Wageningen University, Wageningen, The Netherlands

Received August 5, 2006. In Final Form: November 20, 2006

The adsorption of quaternized poly(vinylpyridine) (QPVP) on controlled pore glass (CPG) size, over the ionic strength range 0.001–0.5 M was found to display nonmonotonic behavior as a function of pore size. Both adsorption kinetics and ionic strength effects deviated dramatically from behavior typical of adsorption on flat surfaces when the ratio of the pore radius R_p to the polymer hydrodynamic radius R_h became smaller than ca. 2. Ionic strength enhancement of adsorption for small pore sizes was observed at much higher salt concentrations than is typical for polycation adsorption on flat surfaces. The amount of polymer adsorbed per unit surface area of glass Γ_A , in 0.5 M NaCl, exhibited a shallow maximum at $R_p/R_h \approx 5$. Since the value of Γ_A for small pore size CPG is strongly depressed by the large surface area, an alternative and more interesting observation is that the amount of polymer adsorbed per gram of CPG, Γ_w , displays a strong maximum when R_p is equal to or slightly smaller than R_h . The efficiency with which QPVP binds anionic micelles to (negatively charged) CPG (grams of surfactant/grams of QPVP) increases strongly with diminishing pore size, indicating that the configuration of polycation bound to small pores favors micelle binding. Since the micelles are larger than small pores, the results indicate that when $R_p < R_h$, adsorbed polycation molecules reside only partially within the pore. The results of this study are supported by simulations of polyelectrolytes within cylindrical cavities.

Introduction

Broad interest in the adsorption of polyelectrolytes onto oppositely charged surfaces has been stimulated over the last decades by its relevance to many areas, including scale inhibition¹ and flocculation and stabilization,² with numerous applications in paper making, water treatment, personal care products, and foods. The subject has most recently been thrust into the limelight by the explosion of interest, both fundamental and applied, in polyelectrolyte multilayers^{3–7} which are typically supported by charged surfaces. In contrast with studies⁸ on the adsorption of neutral polymers in/on confined porous surfaces, nearly all experimental and theoretical studies on polyelectrolyte adsorption address ideal flat surfaces or model colloids with uniform and spherically symmetrical surfaces.

One field in which surface rugosity has not been neglected is pulp and paper making, where a pronounced effort has been made to investigate polycation adsorption on complex surface topography particularly for fibers with nonconfined porous surfaces.⁹ In paper making, polycations are widely used as

additives which by adsorbing on porous pulp fibers improve drainage and fines retention during the formation of fibrous mat.¹⁰ Experiments have focused on polycation adsorption on external fiber surfaces as well as adsorption within the fiber walls and have explored the dependence of the adsorbed amounts on surface charge density, ionic strength, and polymer properties that influence the affinity.¹¹ These studies concluded that initial rapid adsorption is followed by slower penetration into the interior walls resulting in swelling and reformation of the polymer on the fiber surface.¹²

Intermediate between the complex surface topology of fibers and flat surfaces should be porous surfaces with defined geometry, but studies of polyelectrolyte adsorption on such surfaces are remarkably few. Since many of the surfaces relevant to applications are not flat, polyelectrolyte adsorption onto charged fractal surfaces should be of general interest. However, such phenomena present a challenge to the superb techniques that have developed for polyelectrolyte-modified planar surfaces¹³ and also represent a problematic application for the rich theoretical literature so far developed.^{14–17} We present here for the first time to the best of our knowledge a systematic study of polyelectrolyte adsorption on a nonplanar substrate well-characterized with respect to surface charge and porosity.

* To whom the correspondence should be addressed. Mishael: e-mail, mishael@agri.huji.ac.il. Dubin: tel, 1-413-577-4167; fax, 1-413-577-0099; e-mail, dubin@chem.umass.edu.

† Hebrew University of Jerusalem.

‡ University of Massachusetts Amherst.

§ Wageningen University.

(1) Ray, J. M.; Fielder, M. In *Chemicals in the Oil Industry*; Royal Society of Chemistry: London, 1988; pp 87–107.

(2) Russel, W. B.; Saville, D. A.; Schowalter, W. R. *Colloidal Dispersions*; Cambridge University Press: Cambridge, 1989.

(3) Vodouhe, C.; Guen, E. L.; Garza, J. M.; Francius, G.; Dejgnat, C.; Ogier, J.; Schaaf, P.; Voegel, J. C.; Lavallo, P. *Biomaterials* **2006**, *27*, 4149–4156.

(4) Shim, B. S.; Starkovich, J.; Kotov, N. *Compos. Sci. Technol.* **2006**, *66*, 1171–1178.

(5) Porcel, C.; Lavallo, P.; Ball, V.; Decher, G.; Senger, B.; Voegel, J. C.; Schaaf, P. *Langmuir* **2006**, *22*, 4376–4383.

(6) Pettersson, G.; Høglund, H.; Wågberg, L. *Nord. Pulp Pap. Res. J.* **2006**, *21*, 122–128.

(7) Meyer, F.; Ball, V.; Schaaf, P.; Voegel, J. C.; Ogier, J. *Biochim. Biophys. Acta* **2006**, *1758*, 419–422.

(8) Grull, H.; Shaulitch, R.; Yerushalmi-Rozen, R. *Macromolecules* **2001**, *34*, 8315–8320.

(9) Wågberg, L. *Nord. Pulp Pap. Res. J.* **2000**, *15*, 586–597.

(10) Alinec, B.; Vanerek, A.; van de Ven, T. G. M. *Ber. Bunsen-Ges.* **1996**, *100*, 954–962.

(11) Lafuma, F. *Paper Chemistry*, 2nd ed.; Chapman & Camp: Glasgow, 1996; Vol. 4.

(12) Solberg, D.; Wågberg, L. *Colloids Surf., A* **2003**, *219*, 161–172.

(13) Tripathy, S. K.; Kumar, J.; Nalwa, H. S. *Handbook of Polyelectrolytes and their Applications*; American Science Publishers: Stevenson Ranch, CA, 2002; Vol. 1–3.

(14) Dobrynin, A. V.; Rubinstein, M. *Prog. Polym. Sci. (Oxford)* **2005**, *30*, 1049–1118.

(15) Li, Z.; Wu, J. J. *Phys. Chem. B* **2006**, *110*, 7473–7484.

(16) Dobrynin, A. V.; Deshkovski, A.; Rubinstein, M. *Phys. Rev. Lett.* **2000**, *84*, 3101–3104.

(17) Fleer, G. J.; Cohen Stuart, M. A.; Scheutjens, J. M.; Cosgrove, T.; Vincent, B. *Polymers at Interfaces*. Chapman & Hall: London, 1993.

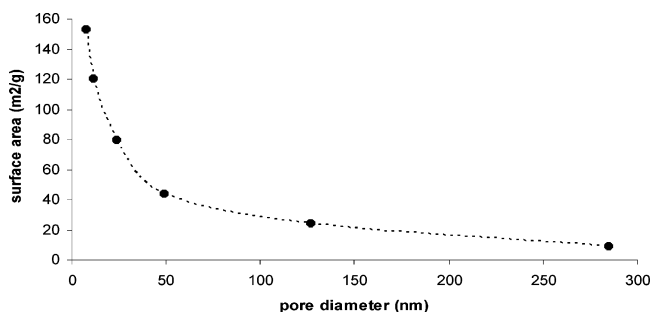


Figure 1. CPG surface area as a function of CPG pore diameter.

Recently, polyelectrolytes adsorbed on porous materials (typically polycations on porous glass) have been used for separations of proteins^{18–20} and trace metals.²¹ In our previous study, controlled pore glass (CPG)–polycation composites were used to immobilize micelles in order to remove organic pollutants from water.²² In the course of that study, we observed somewhat surprisingly, strong adsorption of polycation on CPG with mean pore diameter ($2R_p$) almost half the polycation hydrodynamic diameter ($2R_h$). Other atypical results were very slow adsorption kinetics, linear adsorption isotherms, and high adsorption at high ionic strength. These results point to an incomplete understanding of polyelectrolyte adsorption on oppositely charged nonplanar surfaces, with particular focus on the effects of the key variables: pore size, polymer dimensions, ionic strength, and polymer concentration. In order to probe the effects of the aforementioned variables on both the kinetics and equilibria of adsorption, we examined the adsorption of quaternized poly(vinylpyridine) (QPVP) on CPG with pore sizes ranging from 7.5 to 285 nm. The experimental results, taken together with modeling, show that polyelectrolyte adsorption occurs at $R_p/R_h < 1$ by partial confinement of the chain with the interesting results of both increased adsorption, and, in our case, enhanced micelle uptake. In this regard, micelles—well-characterized with respect to charge and size—may serve as models for other nanoparticles that are amenable to polyelectrolyte anchoring to charged surfaces. These findings suggest that the judicious choice of R_p/R_h could maximize the efficiency of polyelectrolyte-mediated binding, e.g., maximize the amount of protein bound per mass of substrate in applications such as enzyme immobilization.^{20,23,24}

Materials and Methods

Materials. CPGs with mean pore diameters of 7.5, 8.1, 11.5, 24, 49, and 285 nm (henceforth designated as CPG7.5, etc.) and corresponding surface areas of 153, 180, 120, 80, 44, and 9.2 m²/g, were purchased from Millipore (Lincoln Park, NJ). All particle sizes are 200/400 mesh, with the sole exception of CPG7.5 (100/200 mesh); results presented below suggest that mesh size does not strongly influence adsorption per unit surface area. Figure 1 shows the correlation between surface area and pore size. Fitting of this curve shows that the area is proportional to the 2.2 power of the radius which is consistent with a fractal character (neither an idealized spherical nor cylindrical cavity) and with other studies of CPG.²⁵

(18) Tsargorodskaya, A.; Nabok, A. V.; Ray, A. K. *Nanotechnology* **2004**, *15*, 703–709.

(19) Volodkin, D. V.; Larionova, N. I.; Sukhorukov, G. B. *Biomacromolecules* **2004**, *5*, 1962–1972.

(20) Wang, Y.; Dubin, P. L. *J. Chromatogr., Sect. A* **1998**, *808*, 61–70.

(21) Stair, J. L.; Holcombe, J. A. *Microchem. J.* **2005**, *81*, 69–80.

(22) Mishael, Y. G.; Dubin, P. L. *Environ. Sci. Technol.* **2005**, *39*, 8475–8480.

(23) Gergely, C.; Bahi, S.; Szalontai, B.; Flores, H.; Schaaf, P.; Voegel, J. C.; Cuisinier, F. J. G. *Langmuir* **2004**, *20*, 5575–5582.

(24) Ladam, G.; Schaaf, P.; Decher, G.; Voegel, J. C.; Cuisinier, F. J. G. *Biomol. Eng.* **2002**, *19*, 273–280.

(25) Gelb, L. D.; Gubbins, K. E. *Stud. Surf. Sci. Catal.* **2000**, *128*, 61–69.

CPG was washed for 1 h in 1% sodium dodecyl sulfate (SDS), pH 9.5, NaOH solution, and then rinsed with Milli-Q water and dried at 50 °C overnight. Poly(4-vinylpyridine) quaternized with methyl iodide (QPVP) “Reiline 450 quat”, nominal molecular weight 700k, was from Reilly Industries (Indianapolis, IN). SDS was purchased from Fisher Scientific (FairLawn NJ). Triton X-100 (TX100) and acetonitrile were from Aldrich (Milwaukee, WI). Milli-Q water was used throughout this study.

Dynamic Light Scattering (DLS). Solutions of TX100/SDS (20 mM total surfactant concentration, SDS mole fraction $Y = 0.35$ and 0.5 M NaCl) and QPVP (5 g/L) (pH = 9.5 and 0.01–0.5 M NaCl) were prepared. DLS measurements were made after sample filtration (0.2 μ m) using a Malvern Instruments (Southborough, MA) Zetasizer Nanosystem. Mean apparent translational diffusion coefficients were determined by fitting the autocorrelation functions using the program “general modes”, similar to CONTIN, and the apparent hydrodynamic radii were calculated from Stokes law as $2R_h = 12.4$ nm for the polymer and 24 nm for the micelles (0.5 M NaCl).

QPVP Adsorption on CPG. To follow adsorption kinetics, 5 mL of QPVP (5 or 10 g/L) in 0.5 M NaCl adjusted to pH 9.5 was added to 0.375 g of CPG, CPG7.5, -8.8, and -285 and rocked for 2 h. At times varying between 1 min and 2 h, 0.1 mL aliquots were collected after CPG settling, and QPVP concentrations were determined by UV (256 nm) via a standard calibration curve. For equilibrium studies, 4 mL of QPVP (0.5–20 g/L) in NaCl (0.01–4 M) adjusted to pH 9.5 was added to 0.3 g of CPG and rocked for 4 days. The concentration of QPVP in the supernatant was determined after centrifugation (3000 rpm, 20 min) and again after washing with 4 mL of Milli-Q water. The amount of QPVP adsorbed (i.e., retained after washing) per unit surface area (Γ) was calculated by subtraction of the quantities removed from the original mass.

Micelle Adsorption on CPG–QPVP. Four milliliters of TX100/SDS (anionic surfactant mole fraction $Y = [\text{SDS}]/([\text{SDS}] + [\text{TX100}]) = 0.35$) at 20 mM total surfactant concentration, in pH 9.5, 0.5 M NaCl, was added to CPG to which QPVP had been adsorbed. The samples were rocked overnight and centrifuged (3000 rpm 0.5 h), and the concentration of TX100 in the supernatant was measured by UV (224 nm). An additional measurement was made for a 4 mL deionized (DI) water rinse, and the sum of the results for supernatant and rinse was used to determine the total quantity of removable TX100. This was then used to calculate the total mass of micelle bound, assuming no change in Y upon adsorption, as indicated by previous studies.²²

Zeta-Potential Measurements. Untreated CPG49 or CPG49 with different levels of adsorbed QPVP (1–5 g/L added) or CPG49 treated first with QPVP (5 g/L) and then with mixed micelles (as described above) was rinsed and oven-dried overnight. The modified CPG was resuspended in 0.1 M NaCl and the mobility/zeta potential measured using a Malvern Instruments (Southborough, MA) Zetasizer Nanosystem. The rate of settling did not preclude stable or reproducible measurements.

Monte Carlo Free Energy Estimates. Monte Carlo simulations of a single polyelectrolyte chain in a nanopore were performed in the canonical ensemble using the Metropolis algorithm. The chain consisted of $N = 100$ segments of average segment length $l = 1.5$ nm and was enclosed in a square box with sides $L = 200$ nm. Periodic boundary conditions were used, and interactions were truncated using the minimum image convention. Chain connectivity was modeled using harmonic springs. Electrostatic monomer–monomer interactions are taken into account via an effective potential of interaction $V_{\text{int}}(r)$. Interactions between polyelectrolyte monomers and the cylindrical nanopore (along the z -axis) are taken into account via a confinement potential that depends on the distance $(x^2 + y^2)^{1/2}$ to the z -axis

$$H = \frac{1}{2} K \sum_{i=1, N-1}^{N-1} |(\mathbf{r}_{i+1} - \mathbf{r}_i) - l| + \sum_{i \neq j} V_{\text{int}}(|\mathbf{r}_i - \mathbf{r}_j|) + \lambda \sum_{i=1, N} V_{\text{conf}}((x_i^2 + y_i^2)^{1/2}) \quad (1)$$

The parameter λ is needed for free energy estimates as discussed below. The value used for the stretching elastic constant was $K_{\text{stretch}} = 10 \text{ kT/nm}^2$. For the effective monomer–monomer potential of interaction we use the Debye–Hückel expression, plus a term to account for purely steric repulsion

$$\frac{V_{\text{int}}(r)}{kT} = l_B \frac{\alpha_{\text{mon}}^2 \exp(-\kappa r)}{r} + \left(\frac{2R}{r}\right)^{12} \quad (2)$$

where $l_B = e^2/\epsilon kT = 0.7 \text{ nm}$ is the Bjerrum length, e is the elementary charge, ϵ is the permittivity of the aqueous solvent, and kT is thermal energy. The Debye screening length is $\kappa^{-1} = (8\pi l_B n_s)^{1/2}$, where n_s is the number density of excess added monovalent electrolyte.

The monomer radius is $R = 1.0 \text{ nm}$, and the monomer (point) charge $\alpha_{\text{mon}} = 1.0$ is in units of elementary charges e . Here we consider only the steric repulsion between monomers and the nanopore surface, for which we use

$$V_{\text{conf}}^{\text{steric}}(\mathbf{r}) = \begin{cases} 0 & (x^2 + y^2)^{1/2} < R_p \\ V_{\text{steric}}(1 + (x^2 + y^2)^{1/2}/L_{\text{box}}) & (x^2 + y^2)^{1/2} > R_p \end{cases} \quad (3)$$

where $R_p = 10 \text{ nm}$ is the pore radius and the monomer position is $\mathbf{r} = (x, y, z)$. This particular form, with $V_{\text{steric}} = 10 \text{ kT}$, was found to be efficient in the thermodynamic integration procedure for determining free energies. The free energy ΔF of transferring a single chain from a bulk solution to the nanopore is related to experimentally observable partition coefficients P in a dilute system

$$P = \exp(-\Delta F/kT) \quad (4)$$

Free energies are computed using thermodynamic integration

$$\frac{\partial(F_{\text{bulk}} - F_{\text{pore}})}{\partial\lambda} = \left\langle \sum_{i=1,N} V_{\text{conf}}((x_i^2 + y_i^2)^{1/2}) \right\rangle_{\lambda} \quad (5)$$

Switching on the confinement potential reduces the translational entropy of the chain, and this contribution should not be included in ΔF

$$\Delta F = (F_{\text{bulk}} - F_{\text{pore}}) - kT \ln(V_{\text{box}}/V_{\text{pore}}) \quad (6)$$

Trial moves consist of local moves (small translations of monomer positions), reptation moves, as well as large translations and rotations of the entire chain. Single runs consisted of 10^6 MC cycles on equilibrated initial configurations. For a single free energy estimate we typically used 25 single runs, for values of λ between 0 and 1.

Results and Discussion

Kinetics of Adsorption for Small ($R_p/R_h < 1$) and Large ($R_p/R_h > 10$) Pores. The time dependence (0–120 min) of QPVP adsorption on CPG8 and CPG285 as Γ_A (mg of QPVP/m²) is shown in Figure 2B. Figure 2A presents Γ_w as mg of QPVP/g of CPG to emphasize the large capacity of the small pore size glass.

For CPG8, Γ_A approaches its equilibrium value after 48 h (results not shown) as was also observed for CPG7.5.²² Such an equilibration time is substantially longer than those typical for polycations on negatively charged surfaces. Equilibrium times of a few minutes have been reported for the adsorption of QPVP^{26,27} and cationic polyacrylamide²⁸ on nonporous silica and for the adsorption on carboxymethylated cellulosic pulp of 3,6-ionene.²⁹ On the other hand, adsorption kinetics on CPG285 are similar to those reported for nonporous surfaces. In agreement

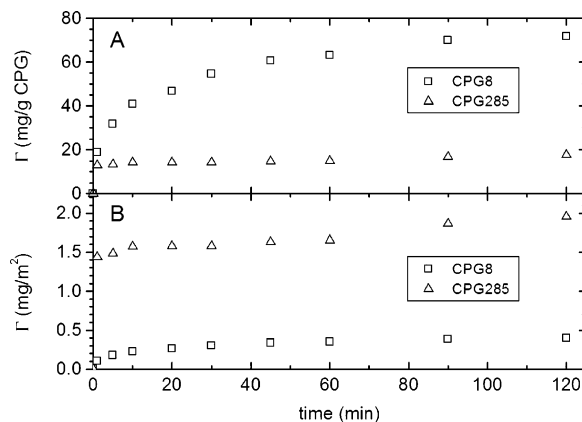


Figure 2. QPVP (10 g/L) adsorption at pH 9.5 and 0.5 M NaCl, as a function of time on CPG8 (□) and CPG285 (Δ). QPVP adsorption expressed as (A) mg/g CPG and (B) mg/m² CPG.

with our results, Grull et al.⁸ reported almost instantaneous adsorption of poly(ethylene oxide) on CPG89 and considerably slower adsorption on CPG8 (20 h). In these cases we can assume that CPG with pore diameters $> 80 \text{ nm}$ are essentially nonporous. Assuming that the initial adsorption is diffusion-limited,²² the polymer reaches porous and nonporous surfaces at the same rate, but porous surfaces evidently provide kinetic obstacles to ultimate equilibrium contacts.

Previously we noted the adsorption of QPVP when $R_p/R_h = 0.60$ and suggested a bound configuration with partial confinement of the chain within the pore.²² The segmental adsorption energy leads to an overall gain in free energy that can compensate for the unfavorable loss of chain entropy and the unfavorable contribution of intrapolymer repulsion. This entropically unfavorable quasi-compressed configuration could be compensated by the enhanced electrostatic interaction between the pore cavity and the entrapped polycationic segments. The process by which the polymer chain attains this particular configuration could also explain the slow kinetics of QPVP adsorption for $R_p/R_h < 1$. In summary we propose that polycation adsorption includes rapid diffusion-controlled binding to the surface followed by slow reorganization with partial pore penetration.

Concerning the larger Γ_A (mg of QPVP/m²) of CPG285 than of CPG8, Grull et al.,⁸ studied the adsorption of poly(ethylene oxide) in/on CPG and stated that the confinement of chains in small pores limits the maximal loops and tail size, leading to a value of Γ_A much lower for confined cases. However, as mentioned above, Γ_w (mg of QPVP/g of CPG) emphasizes the large capacity of the small pore size glass.

Equilibrium Adsorption Isotherms. Adsorption isotherms of QPVP (0–20 g/L in 0.5 M NaCl, pH 9.5) on CPG7.5,²² CPG8, CPG49, and CPG250 are shown in Figure 3 as the dependence of Γ_A on the concentration of free QPVP. Adsorption isotherms for CPG49 and CPG285 behave typically, reaching a plateau at saturation, in contrast to the data for the small pore sizes. These glasses also show small initial slopes, indicating lower QPVP affinity. Shin et al.³⁰ have discussed how a reduction in contacts between polyelectrolyte segments and silica leads to a decrease in initial slope of the isotherm with a shift of plateau to higher polymer concentrations; the isotherms for CPG7.5 and CPG8 show an extreme example of this effect, which arises here from partial exclusion. Plotting Γ_A should remove any effect due to

(26) Hoogeveen, N. G.; Stuart, M. A. C.; Fleer, G. J. *J. Colloid Interface Sci.* **1996**, *182*, 133–145.

(27) Sukhishvili, S. A.; Granick, S. *J. Chem. Phys.* **1998**, *109*, 6861–6868.

(28) Oedberg, L.; Sandberg, S.; Welin-Klintstroem, S.; Arwin, H. *Langmuir* **1995**, *11*, 2621–2625.

(29) Waagberg, L.; Oedberg, L.; Lindstroem, T.; Aksberg, R. *Colloids Surf.* **1988**, *31*, 119–124.

(30) Shin, Y.; Roberts, J. E.; Santore, M. M. *Macromolecules* **2002**, *35*, 4090–4095.

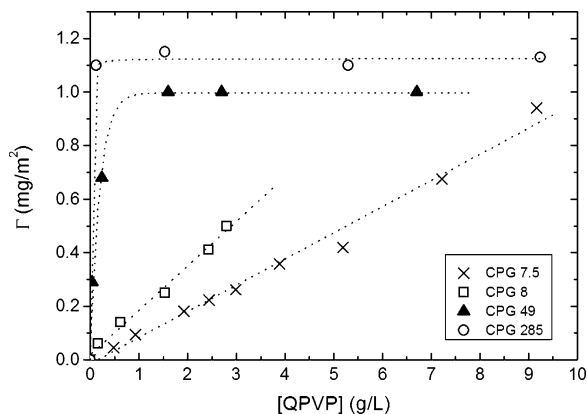


Figure 3. Adsorption isotherm of QPVP (0.5 M NaCl, pH 9.5) on CPG with pore diameters of 7.5, 8, 49, and 285 nm.

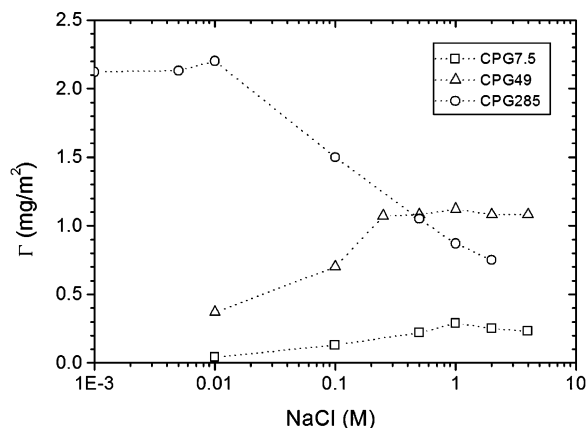


Figure 4. QPVP adsorption on CPG7.5, CPG49, and CPG285 from 0.001 to 4 M NaCl.

the smaller particle size of CPG7.5, so that the difference between the two glasses can be attributed to the differences in pore size.

Effect of Ionic Strength. Equilibrium adsorption from 5 g/L QPVP onto CPG ($2R_p = 7.5, 49, \text{ and } 285 \text{ nm}$) was measured at pH 9.5 over the ionic strength range 0.01–4 M NaCl, with the results shown in Figure 4. Many studies have reported a maximum in Γ_{equ} with respect to I for adsorption on flat surfaces^{27, 31} and on wood fibers.¹² This maximum is generally accounted for by different behavior in low and high salt regimes. In the first case, corresponding to large Debye lengths κ^{-1} , interchain and intrachain repulsions that would tend to reduce coverage are screened by added salt leading to a slight increase in Γ_{equ} . Subsequent increase in I screens more short-range favorable interactions between polymer segments and the charged surface, and therefore Γ_{equ} decreases (for recent reviews on polyelectrolyte adsorption see refs 14 and 32). Consistent with these competing effects, Granick et al. observed a maximum at $I = 1 \text{ M}$ for $3.5 \times 10^5 \text{ MW}$ QPVP on bare silica at pH 9.2. This result is different from that of our most closely related system, CPG285 which shows no ionic strength enhancement of adsorption. Since ionic strength enhancement of adsorption arises from reduction in repulsions among near by adsorbed chains, this suggests that even the modest curvature of 140 nm radius pores tends to increase the distance between adsorbed chains. It should be noted that distances between chains influence the equilibrium values in Figure 4, while the initial slopes of the isotherms of Figure 3 reflect single-molecule uptake. The onset of adsorption suppression at $\kappa^{-1} \approx 3 \text{ nm}$ here, in contrast to 0.3 nm in ref 25, could

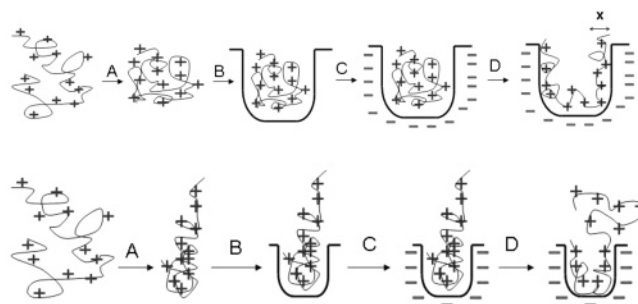


Figure 5. Schematic representation of hypothetical steps in the adsorption of polyelectrolyte into an oppositely charged pore either larger (above) or smaller (below) than the PE: A, compression of the polyelectrolyte to a conformation with a radius of gyration $R_g^* < R_p$; B, insertion of the compressed polyion into a hypothetical discharged pore; C, recharging of the pore; D, reconfiguration of the polycation in response to the intrapore potential. Lower set shows hypothetical steps leading to partial confinement.

indicate that attractive interactions between polycations and the surface are on average more short range in the case of the planar and more highly charged bare silica.

The ionic strength dependence is very different for $R_p < R_h$, as shown by the results in Figure 4 for CPG7.5. For an intuitive explanation, we begin by viewing polyelectrolyte adsorption within such a pore according to the hypothetical sequence of events for the adsorption of a single polyion chain, represented by the upper five images in Figure 5. Step A represents contraction of the chain to dimensions small enough to be accommodated by the pore and involves both intrapolyion segment repulsions and loss of chain configuration entropy. Step B corresponds to insertion into a hypothetical uncharged pore and is equivalent to the steric exclusion effect measured in size-exclusion chromatography. These two steps, which we refer to as “compression” and “confinement”, respectively, are both energetically unfavorable. In step C, charges are returned to the pore and allowed to interact with the polyion without inducing conformational change. In the final step D, the included chain is allowed to rearrange under the influence of the pore potential. The favorable electrostatic interaction energies of steps C and D termed “adsorption” and “reconfiguration”, respectively, more than compensate for A and B. These processes have different I dependencies and hence, in combination, may lead to an overall nonuniform dependence of adsorption on ionic strength. A similar hypothetical sequence culminating in a partially confined polyion, represented by the lower set of images, will be invoked in further discussion of results for the case $R_h/R_p < 1$.

The addition of salt makes step A more favorable: screening reduces intrapolymer repulsion such that compression costs less. At higher coverage, a further favorable effect comes from screening the interpolymer repulsions. Screening has no effect on step B, for which the energy is simply the typical size-exclusion effect, and data obtained by size-exclusion chromatography on CPG elsewhere³³ justify the result for cylindrical pore geometry, i.e.

$$\Delta G = -RT \ln \left[1 - \frac{R_h^*}{R_p} \right]^2 \quad (7)$$

where R_h^* is now the hydration radius of the compressed polycation. Since steps C and D both become less favorable with increase in I , the favorable effect of I for the adsorption of a single chain comes from amelioration of step A alone. A very

(31) Hansupalak, N.; Santore, M. M. *Langmuir* **2003**, *19*, 7423–7426.

(32) Netz, R. R.; Andelman, D. *Phys. Rep.* **2003**, *380*, 1–95.

(33) Dubin, P. L.; Speck, C. M.; Kaplan, J. I. *Anal. Chem.* **1988**, *60*, 895–900.

important point, supported by results to be presented later, is that the identical scenario can be applied to partial confinement of the chain, as depicted in the lower set of images of Figure 5.

Just how much more favorable is step A at high salt than at low salt? Since the early work of Casassa³⁴ on confined ideal polymers, many authors have addressed the impact of confinement on uncharged polymers.³⁵ Scaling theory³⁶ provides simple order-of-magnitude estimates that may also be used for polyelectrolytes. In the limit of strong confinement, the confined polymer may be viewed as a sequence of “blobs” of size R_p with a confinement free energy of approximately kT per blob. The average segment number density ρ_p increases rapidly with decreasing pore radius. Assuming that the blobs have full excluded volume

$$\rho_p \approx \frac{1}{l_K^{5/3} R_p^{4/3}} \quad (8)$$

where l_K is the polymer segment length. For strong confinement, the confinement free energy ΔG is linear in the polymer contour length L

$$\frac{\Delta G}{kT} \approx L \frac{(\beta/l_K)^{1/3}}{R_p^{3/5}} \quad (9)$$

where β is the segment–segment excluded volume. For polyelectrolytes we replace the values of the segment length and segment–segment excluded volume, by ionic strength dependent effective values³⁷

$$l_{K,\text{eff}} \approx \kappa^{-2} l_B^{-1} \\ \beta_{\text{eff}} \approx l_{K,\text{eff}}^2 \kappa^{-1} \approx \kappa^{-5} l_B^{-2} \quad (10)$$

Substituting these in (9) gives a scaling estimate for the ionic strength dependence of the confinement free energy of polyelectrolytes in pores with nonadsorbing walls steps (A + B) in Figure 5

$$\Delta G \propto \kappa^{-1} \propto n_s^{-1/2} \quad (11)$$

If excluded volume is neglected for relatively short chains, the remaining electrostatic chain stiffening effect leads to an even stronger dependence of $\Delta G \propto n_s^{-1}$. Clearly, the confinement free energy decreases strongly with salt. Perhaps first among the various nonideal effects to be additionally considered is the strong increase in the local segment density with confinement. For pores with radii $O(10 \text{ nm})$ at low ionic strengths, one quickly approaches the limit of strongly interacting polyelectrolytes (“salt-free regime”) where the scaling picture for polyelectrolytes with excess electrolytes breaks down.

In order to obtain more accurate estimates down to low ionic strengths for the confinement free energy (ΔG for step A), we performed preliminary Monte Carlo free energy calculations for a polyelectrolyte chain of $N = 100$ segments of segment length $l_K = 1.5 \text{ nm}$, each carrying a single elementary charge, confined within a cylindrical cavity. In the unconfined state, the gyration radius decreases from $R_g = 20$ to 9 nm between $I = 0.001 \text{ M}$ and $I = 1$. Confinement begins to play a role when polymer is confined in a pore with radius $R_p = 10 \text{ nm}$. At the lowest ionic strength of $I = 0.001 \text{ M}$, the gyration radius parallel to the pore

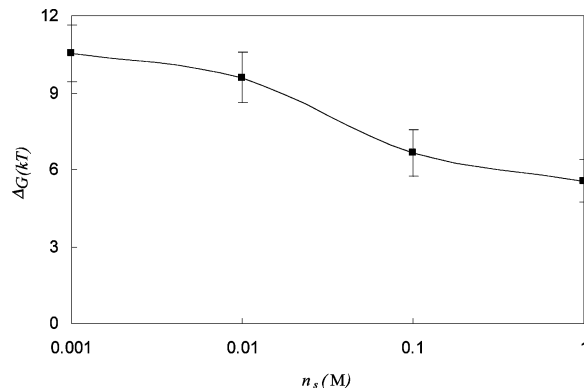


Figure 6. Monte Carlo free energy estimates for the confinement free energy of a polyelectrolyte coil in a nanopore as a function of ionic strength. The polyelectrolyte consists of 100 segments of 1.5 nm length, each carrying a single elementary charge. Pore radius is 10 nm.

axis is $R_{g,z} = 23 \text{ nm}$, whereas the gyration radii in the x and y directions (perpendicular to the pore axis) are $R_{g,x} = R_{g,y} = 3.4 \text{ nm}$. Thus, at the lowest ionic strength, the polyelectrolyte coil adopts a drastically stretched configuration. As is shown in Figure 6 the confinement free energy ΔG for this particular pore/polymer combination is significant at all I , but the decrease of ΔG with increasing ionic strength ($6 kT$ for a single coil) is very significant. At low I , ΔG appears to level off in Figure 6.

Clearly it would be desirable to also perform extensive computer simulations for the steps C and D of Figure 5, but this would imply lengthy simulations for a significantly larger parameter space. Also, for strong adsorption, the simple MC moves that we employ here would probably not lead to proper equilibration. Therefore, we leave such more difficult simulations for future work and only discuss the qualitative aspects of the remaining steps C and D. Salt decreases the favorable energy of these steps, but at different length scales. For the first adsorption step C, the length scale is up to R_g^* , but after reconfiguration brings polycation segments close to the wall of the pore (step D), the length scale x applies.

In order to account for the equilibrium values of Γ in Figure 4, it is necessary to consider not only the interactions of the polyion with the pore described in the last pages but also interactions between nearby adsorbed chains. Thus, the addition of salt promotes adsorption at low I both by facilitating compression and by reducing interpolyion repulsions. For smaller pores, the first effect is dominant; for the largest pore, it disappears. The length scale of the interpolyion effect is larger than the length scale of the compression effect. This is why the regime of salt enhancement (positive $d\Gamma/dI$) extends to larger values of I for smaller pores (compression dominated) in Figure 4. An unfavorable effect of salt for adsorption can begin at $x < \kappa^{-1} < R_g$ (step C), followed by a stronger salt effect at high salt when $\kappa^{-1} < x$ (step D). The relative importance of the various terms A–D is determined by parameters such as the pore and polyelectrolyte charge densities and the ratio of the polyelectrolyte size to the pore size. For CPG285, suppression of adsorption (inverse dependence of Γ_{equ} on I) begins to take place at $I > 0.01 \text{ M}$. For CPG7.5, the unfavorable effect of salt is only seen for $I > 1 \text{ M}$. This could arise from extension of positive $d\Gamma/dI$ to higher salt due to more severe compression or because a higher ionic strength is required to suppress the high potential within pores of high curvature (see below) leading to retardation of the regime of negative $d\Gamma/dI$. CPG49 represents an intermediate case, with a gradual transition from enhancement to suppression at $I > 0.3 \text{ M}$, corresponding to $\kappa^{-1} \leq 0.3 \text{ nm}$.

(34) Casassa, E. F.; Tagami, Y. *Macromolecules* **1969**, *14*.

(35) Teraoka, I. *Prog. Polym. Sci. (Oxford)* **1996**, *21*, 89–149.

(36) de Gennes, P. G. *Scaling Concepts in Polymer Physics*; Cornell University Press: Ithaca, NY, 1979.

(37) Odijk, T. *Macromolecules* **1979**, *12*, 688–693.

The increase in electrostatic potential due to the charged pore surface inside pores of small radius has been addressed by Lin and Deen.³⁸ This work was elaborated on by Park et al.³⁹ who included intrachain repulsion in a heuristic way. The curvature effect is part of term (C): it favors adsorption in pores over adsorption to flat interfaces. Although the effect is most pronounced for pores that are narrow with respect to the screening length ($\kappa R_h < 1$), it might still contribute to some extent for CPG49 and CPG7.5 and explain why for these cases there is no decrease in adsorption at high salt. The description of this and other effects described above is also applicable to a process in which only part of the polyion is confined within the pore. Such a configuration minimizes the penalty of compression while maximizing the energy gain of adsorption and is consistent with the results discussed next, when adsorbed polyion is in turn used to facilitate binding of an object unable to enter the pore directly for both electrostatic and steric reasons.

Micelle Binding to CPG–QPVP. In previous work,²² polycations functioned as bridges, adsorbing anionic micelles to negatively charged glass or sand. While it might be thought that polycations could induce micelle distintegration or deformation, several observations serve to indicate the integrity of SDS/TX-100 micelles bound to PDADMAC. (1) Micellar solubilization by complexes, either in free solution or as coacervates, is quantitatively no different from that of free micelles.⁴⁰ (2) Cryo-TEM of these complexes show micelle size unaltered (within the limits of resolution) compared to polycation-free solution.⁴¹ (3) The correlation between the surface charge densities or surface potentials measured for polycation-free micelles and the ionic strength at the onset of binding, and its good agreement with theory⁴² (and references cited therein), is difficult to explain if micelle structures are altered upon binding. The uptake of these large colloidal particles onto CPG–QPVP provides an indication of the amount and configuration of adsorbed polycations. To investigate correlation between adsorption of polycation and subsequent binding of anionic micelles, we measured electrophoretic mobilities of CPG, CPG–QPVP, and CPG–QPVP–micelles. Zeta potentials obtained for bare CPG49 and for CPG49 brought to equilibrium with 1, 2.5, and 5 g/L QPVP were -23 , -13 , $+3$, and $+9.5$ mV, respectively. This indicates that the negative potential of the CPG decreases with the adsorption of the polycation, attaining charge reversal at intermediate QPVP loading, consistent with the adsorption modes suggested above. When anionic/nonionic micelles were added to CPG49 pre-equilibrated with 5 g/L QPVP, a second charge reversal was seen, from $+9.5$ to -9 mV. These results confirm the immobilization of excess negative micelles onto a negatively charged porous surface through the intermediacy of the bound polycation. However, the effects of pore size on both QPVP adsorption and subsequent micelle binding described below were unexpected and gave further insight into polycation configuration.

CPG8, CPG11.5, CPG24, CPG49, and CPG285 treated with QPVP at 5 g/L, $I = 0.5$ M, were equilibrated with mixed micelles ($I = 0.5$ M) with results shown in Figure 7. It is noteworthy that data for the different pore sizes conform to a single curve even though the results were obtained from CPG with different particle sizes. Expressed in the usual way, Γ_{equ} shows a weak maximum around $R_p = 50$ nm (Figure 7B). When expressed as Γ_w (mg of

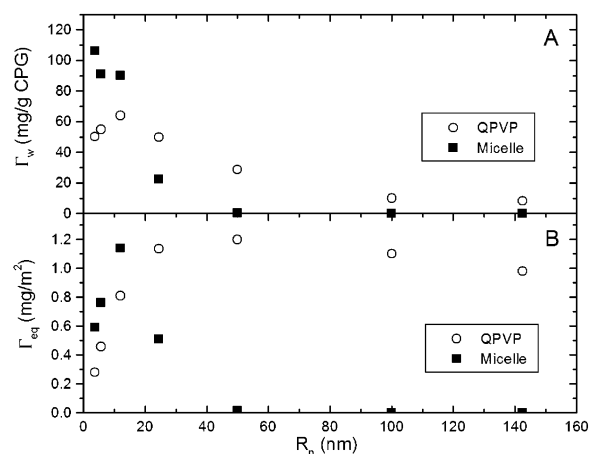


Figure 7. (A) QPVP adsorption (mg/g CPG) on CPG and micelle binding (mg/g CPG) to CPG–QPVP as a function of CPG pore diameter. (B) Data of part A reported as adsorption per unit surface area of CPG.

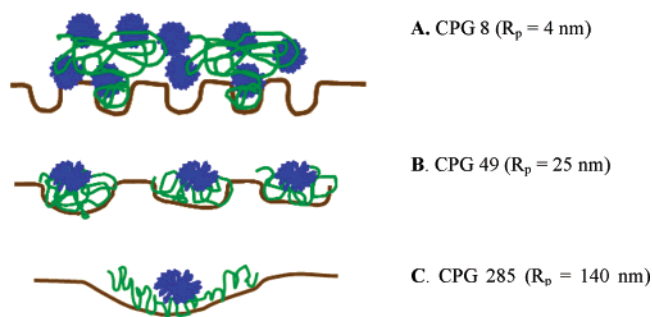


Figure 8. Micelle binding to QPVP adsorbed with different configurations on (A) CPG8, (B) CPG49, and (C) CPG285.

QPVP/g of CPG), one sees a well-defined maximum at $R_p = 12$ nm. The decrease in Γ_w at high pore diameters can be simply explained by the decrease in surface area, while the initial increase in Γ_w may be explained by the increase in pore accessibility. The balance between pore accessibility and surface area leads to the maximum in Γ_w , but it is notable that this maximum occurs when $R_p = R_h$, where steric considerations (see eq 7) would predict obstruction of permeation. However, micelle binding, Φ (mg of surfactant/g of CPG) (Figure 7A), does not correlate with Γ_w and in fact decreases dramatically with increasing pore size. The hydrodynamic radius of the micelles is about 8–9 nm.²² Such micelles cannot permeate the pores for low R_p but must be adsorbed by polymer present outside of pores, as schematically represented in Figure 8.

The ratio between Φ and Γ_w (g of surfactant/g of QPVP) is a measure of the efficiency of micelle binding by the polycation, and the data in Figure 7B reveal that this ratio increases rapidly as pore size diminishes, particularly for $R_p < R_h$. The inescapable conclusion is that the configuration of adsorbed polycations favors micelle binding when pores are small compared to polymer. The most reasonable explanation is that much of the adsorbed polymer then remains outside of the pore as depicted in Figure 8A. Here, the penalty of compression is reduced by allowing part of the polyelectrolyte chain to remain outside of the pore, while the rest of the chain contributes to the favorable energy of adsorption. This configuration is clearly optimal in providing for subsequent binding of anionic micelles. The ineffectiveness of QPVP-treated CPG285 for micelle uptake is probably due to adsorption of the polycation on this nearly flat surface in trains which fail to provide sites for micelle adsorption (perhaps failing to achieve charge

(38) Lin, N. P.; Deen, W. M. *Macromolecules* **1990**, *23*, 2947–2955.

(39) Park, P. J.; Chun, M. S.; Kim, J. J. *Macromolecules* **2000**, *33*, 8850–8857.

(40) Sudbeck, E. A.; Dubin, P. L.; Curran, M. E.; Skelton, J. J. *Colloid Interface Sci.* **1991**, *142*, 512–17.

(41) Swanson-Vethamuthu, M.; Dubin, P. L.; Almgren, M.; Li, Y. *J. Colloid Interface Sci.* **1997**, *186*, 414–419.

(42) Zhang, H.; Ohbu, K.; Dubin, P. L. *Langmuir* **2000**, *16*, 9082–9086.

reversal). On the other hand, the curvature of CPG 285 pores (Figure 8C), while not great enough to lead to partial confinement of the chain as represented in parts A and B of Figure 8, may tend to separate adsorbed chains, and the resultant diminution in interpolyion repulsion can explain the absence of an increase in Γ_{equ} with salt for CPG285 in Figure 4. For small pores, QPVP adsorption per unit surface area is low, but the loading (g of QPVP/CPG) is high. Furthermore, the unique configuration of QPVP on CPG with small pore diameters, in which polycation is partially confined within the pore, leaves an array of unconfined accessible segments available for binding.

Conclusions

The adsorption of a polycation on CPG porous glass changes dramatically as the pore size is diminished and attains dimensions smaller than those of the polymer; i.e., $R_p/R_h < 1$. Specifically, equilibrium adsorption is attained much more slowly, adsorption isotherms become linear, and the effect of ionic strength on Γ also changes markedly. These results are in part explained by simulations of polyelectrolytes confined in nonadsorbing cylindrical nanopores. The amount of adsorbed polymer

per surface area of glass exhibits a shallow maximum near $R_p/R_h \approx 4$, but the amount of adsorbed polymer per gram of glass exhibits a maximum near $R_p/R_h = 1$. When the polycation-coated glass is used to adsorb surfactant micelles, the mass of adsorbed surfactant per unit mass of glass increases without limit with decreasing R_p , indicating that the efficiency of adsorbed polycation for micelle uptake is largest when pores are smaller than the polymer; i.e., the configuration of polymer bound to small pores favors the absorption of large micelles. The implication that the polycations are partially confined to pores was rationalized by a model in which the favorable electrostatics of partial confinement in a small oppositely charged pore outweighs the penalty of polyion compression. It would be useful to generalize these findings to other situations in which polycations are used to bind, e.g., proteins to nonplanar surfaces.

Acknowledgment. Support from the Israeli Council for Higher Education, Bekura postdoctoral fellowship (Y.G.M.), is acknowledged.

LA062314R